

The influence of chromium and molybdenum on the repassivation of nickel-chromium-molybdenum alloys in saline solutions

N. Ebrahimi,  M. C. Biesinger,  D. W. Shoesmith  and J. J. Noël* 

The electrochemical properties and compositions of passive, transpassive, and re-formed passive oxides on the Ni-Cr-Mo alloys C22 (high Cr/low Mo) and HYBRID BC1 (low Cr/high Mo) have been studied in 5.0M NaCl solutions. At low potentials in the passive region, the oxide was less resistive on BC1 compared to C22, possibly due to the influence of Mo in increasing the number of defects in the oxide. At higher potentials in the passive region, both alloys exhibited similar behaviours and composition of oxide films. Under transpassive conditions, the Cr^{III} barrier layer (dominantly Cr₂O₃) was destroyed on both alloys, with a greater accumulation of Mo^{VI}/Mo^V on the BC1 than on the C22 alloy. Improved passivity was achieved for both alloys on returning to potentials in the passive region. This appears to be due mainly to the re-formation of the Cr^{III} barrier oxide layer on C22, but to a combination of the reformation of this layer and the accumulation of Mo^{VI}/Mo^V on the BC1. Copyright © 2017 John Wiley & Sons, Ltd.

Keywords: molybdenum; passive film; repassivation; surface characterization

Introduction

Ni-Cr-Mo alloys exhibit exceptional corrosion resistance under extreme exposure conditions.^[1–5] This resistance is attributed to the formation of a stable passive film whose compositional and electrical properties have been investigated using surface analytical methods^[1–5] and electrochemical impedance spectroscopy (EIS).^[6–9] This film is only nanometres thick and grows with a dual layer structure comprising an inner Cr-Ni layer and an outer Mo-enriched layer. In addition, these alloys are homogeneous in composition, free of intermetallic precipitates, and have a large proportion of symmetrical (Σ 3) low-energy grain boundaries.^[10,11] If these alloys are to suffer localized corrosion, the most likely form appears to be crevice corrosion,^[12–19] with initiation requiring a potential excursion into the transpassive region during which the Cr^{III} barrier layer is destroyed by oxidation to the more soluble Cr^{VI} state. The subsequent accumulation and distribution of corrosion damage has been found to be very dependent on alloy composition^[19] with complete repassivation difficult to achieve.^[18]

In this paper, the properties of the passive film on the C22 (high Cr/low Mo) and HYBRID BC1 (low Cr/high Mo) (hereafter called BC1) alloys were compared using EIS experiments in 5M NaCl at pH 7, followed by X-ray photoelectron spectroscopy (XPS) analyses. The influence of a period of crevice corrosion was simulated by potential excursions into the transpassive region, with the primary goal of the subsequent reduction in potential to demonstrate whether the passive state could be subsequently re-established. For the C22 alloy, this study is an extension of our previous EIS investigations,^[9] which were confined to the influence of an increasingly positive potential and did not include an attempt to correlate the impedance behaviour with film compositions determined by XPS.

Experimental

Sample preparation

C22 and BC1 discs with a diameter of 1 cm² (Table 1) were cut from mill-annealed plates supplied by Haynes International, Kokomo, Indiana (USA). The discs were then mounted in a heat-resistant epoxy resin (Dexter Hysol resin EE4183; hardener HD3561) to ensure that only a single disc face, 0.78 cm² in surface area, was exposed to the electrolyte. Prior to each experiment, the exposed surface was wet-polished with SiC papers from 180 to 1200 grit, ultrasonically cleaned for 10 minutes in a 50/50% mixture of ethanol and water, rinsed with Type-I water, and dried with Ar gas.

Electrochemical procedure

A 3-electrode cell, placed in a grounded Faraday cage, was used for electrochemical measurements, with a Pt plate (2.4 cm²) counter electrode and a home-made Ag/AgCl (sat'd KCl) reference electrode (0.197 V vs NHE). All potentials are reported vs this Ag/AgCl electrode. Experiments were conducted in 5M NaCl solutions prepared with Type I water (resistivity = 18 M Ω cm). The pH was adjusted to 7 using HCl and NaOH solutions. An Orion Model 250A pH metre was used to confirm the solution pH. Solutions were sparged with ultra-high purity Ar gas (1 h) before each experiment,

* Correspondence to: J. J. Noël, Department of Chemistry and Surface Science Western, The University of Western Ontario, London, ON, Canada.
E-mail: jjnoel@uwo.ca

Department of Chemistry and Surface Science Western, The University of Western Ontario, London, ON, Canada

Table 1. Chemical composition (wt.%) of the BC1 and C22 alloys

Alloy/Element	Ni	Cr	Mo	W	Fe	C	Co	Mn	Si	S
BC1	62	15	22	-	2	0.01	-	0.25	0.08	-
C22	56	22	13	3	3	0.01	2.5	0.5	0.08	0.2

-, element not detected in analysis.

and sparging was continued throughout the experiment. All measurements were performed at room temperature.

Prior to each experiment, the working electrode was cathodically cleaned at a potential (E) of -1 V for 1 hour. Oxide films were grown at constant values of E using a Solartron 1287 potentiostat, with E increased and the procedure repeated at 0.1 V intervals from -0.8 V up to 0.6 V and then back again to -0.8 V. An EIS measurement was performed at each E using a Solartron 1255 frequency response analyzer. A sinusoidal input potential with an amplitude of 10 mV was applied at 11 individual frequencies per decade from 10^5 to 10^{-3} Hz. Kramers-Kronig transformations were performed on all impedance spectra to ensure their validity.^[20] Data were obtained and analyzed using Corrware, Corrview, Zplot, and Zview software (versions 2 and 3, Scribner Associates).

To determine compositions, oxide films were grown (for 8 h) at potentials of 0 and 0.5 V as E was increased and at 0 V and -0.4 V as E was decreased. To minimize the effect of air exposure on the oxide composition, specimens were cleaned ultrasonically (60 s) and rinsed in water and dried in Ar gas immediately after growth. They were then stored in a small container in a desiccator before XPS analyses were performed.

Surface analyses

X-ray photoelectron spectroscopy analyses were performed with a Kratos AXIS Nova XPS using an Al $K\alpha$ (1486.7 eV) radiation source. The Au 4f_{7/2} metallic Au binding energy (83.95 eV) was used as a reference point for calibration of the instrument work function. Survey spectra and high-resolution spectra were recorded on all samples for the Ni 2p, Cr 2p, Mo 3d, C 1s, and O 1s spectral regions. Commercial CasaXPS software was used to fit the spectra. If required, charging in XPS spectra was corrected by fixing the C–C binding energy in the C 1s spectrum at 284.8 eV.

Results and discussion

Figure 1 shows current densities (i_{Final}) recorded on BC1 after 2 hours of polarization at a series of potentials (E). Although not shown, C22 exhibited similar behaviour.

The current response could be divided into 3 distinct regions:

For $E < -0.6$ V, i_{Final} was negative. In this region, the surface oxide contains a large number of anion vacancies and supports H_2O reduction. As E was increased, the number density of vacancies decreased, leading to a more resistive oxide.^[21,22]

For E in the range -0.6 to 0.2 V, the current was positive and independent of E with the low value typical for a passive film with a low concentration of defects.

For $E > 0.2$ V, i_{Final} increased with increasing E , indicating the onset of transpassivity.

Figure 2 shows EIS (Bode) plots measured on BC1 at one potential in each region, as E was increased and then subsequently decreased. Although not shown, similar spectra were recorded on C22. In region 1 (Figure 2A), 2 time constants were observed. The

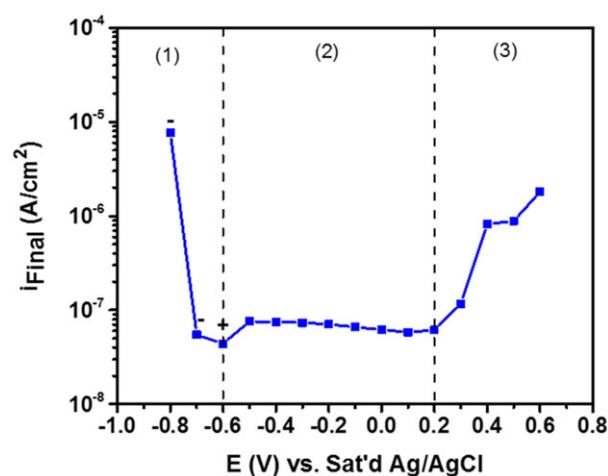


Figure 1. Currents (i_{Final}) recorded as a function of applied E on BC1 in deaerated 5M NaCl. The $-$ sign indicates negative current, and the $+$ sign positive current. Regions 1, 2, and 3 are defined in the text

low frequency response was attributed to the dielectric processes occurring within a thin defective film (ie, an incompletely formed passive film) and the high frequency response to the charge transfer process at the film/solution interface (H_2O reduction). In region 2, Figure 2C,D, only one time constant was required to fit the spectra demonstrating that the interfacial impedance was dominated by the properties of the passive oxide. In region 3, Figure 2E,F, 2 poorly separated time constants were required to fit the spectra.

Depending on whether 1 or 2 time constants were required, one or the other of the electrical equivalent circuits shown in Figure 3 was used to fit the spectra. To account for nonideality in the capacitive responses, constant phase elements (CPE) were used to achieve acceptable fits. The exponent of CPE_f was >0.8 in regions 1 and 3 and >0.9 in region 2. For the high-frequency time constant, the exponent of CPE_{ct} ranged from 0.6 to 0.83.

Attempts to correct for nonideality by converting CPE values to capacitances using the method proposed by Hirschorn et al.^[23] were unsuccessful. Also, while the introduction of a Warburg impedance into the equivalent circuit to account for contributions from diffusion in regions 1 and 3 led to visually improved fits, the accuracy of the fit was not significantly improved. Consequently, since our primary interest is in the properties of the oxide film, only values for the film resistance (R_f) associated with the low-frequency time constant were considered further. These values are plotted in Figure 4 for both alloys. As E was increased from -0.9 V (positive scan), R_f values for BC1 ($R_f(\text{BC1})$) were considerably lower than those for C22 ($R_f(\text{C22})$) up to $E = -0.3$ V, reflecting the earlier formation (on the E scale) of a passive oxide on the high Cr alloy. The lower $R_f(\text{BC1})$ values were consistent with the observations of Betova et al.^[24] and Bojinov et al.^[25] who showed that the presence of Mo in the oxide (presumably as $\text{Mo}^{\text{III}}/\text{Mo}^{\text{IV}}$) altered the kinetics of generation and annihilation of point defects in the oxide on Fe–Cr–Mo alloys, leading to measurably lower film resistances. The decrease in resistance was found to be larger the higher the Mo/Cr ratio in the substrate alloy, consistent with our observations that the low Mo-containing C22 developed a passive oxide more readily than the higher Mo-containing BC1.

For $E \geq -0.3$ V (region 2: the passive region), $R_f(\text{C22})$ was slightly higher than $R_f(\text{BC1})$, as expected given the higher Cr and lower Mo

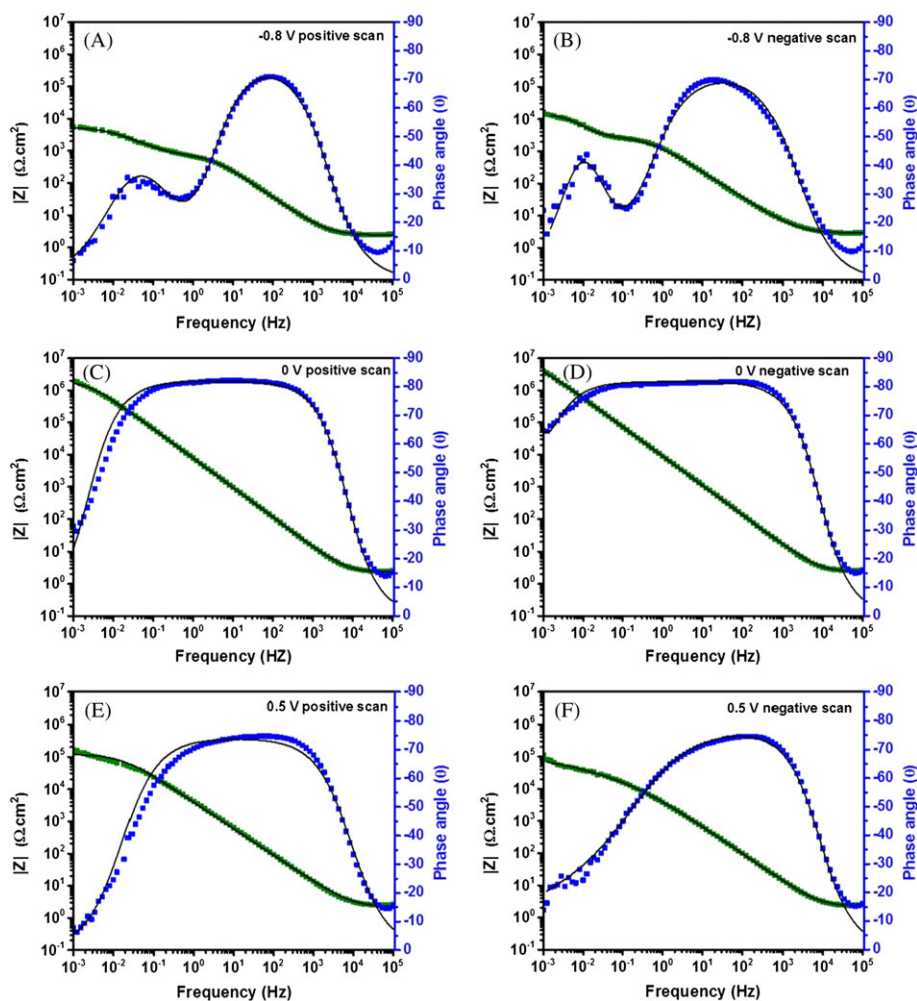


Figure 2. EIS (Bode plots) recorded on BC1 at 3 potentials (E) in 5M NaCl (pH = 7). Scans A, C, and E were recorded as E was increased; scans B, D, and F were recorded as E was decreased. The points indicate the experimental data and the lines the fits of the electrical equivalent circuits in Figure 3

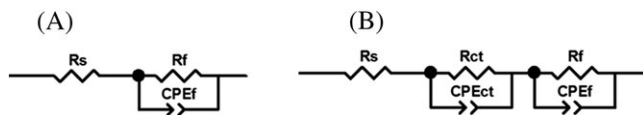


Figure 3. Electrical equivalent circuits used to fit EIS data. CPE_{ct} , constant phase element representing the nonideal capacitance of the alloy/oxide interface; CPE_f , constant phase element representing the non-ideal capacitance of the film; EIS, electrochemical impedance spectroscopy; R_s , solution resistance; R_{ct} , charge transfer resistance at the alloy/oxide interface; R_f , oxide film resistance

content of C22. The subsequent rapid increase in R_f (C22) as E was increased was expected for the potential-driven formation of a passive oxide. For $E \geq 0.2$ V (region 3: the transpassive region), the R_f values are similar for both alloys. This is particularly so for the BC1 alloy for which R_f on the negative scan is an order of magnitude greater than on the positive scan.

Both alloys exhibited higher R_f values on the negative scan than on the positive scan. For BC1, the film resistance remained stable to

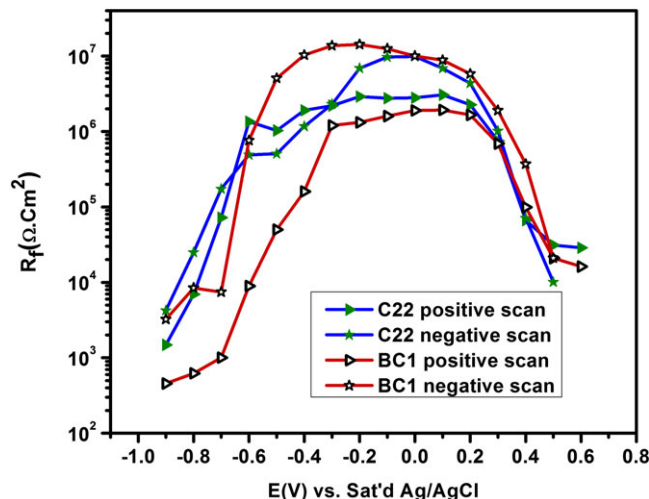


Figure 4. Film resistances (R_f) as a function of applied E on BC1 and C22

$E \sim -0.5$ V while $R_f(\text{C22})$ decreased markedly over the potential range -0.2 to -0.7 V, Figure 4A, suggesting a more defective film was present on this alloy, possibly allowing the reduction of trace amounts of dissolved O_2 in the solution. We have previously observed the reduction of O_2 within this potential range^[26] (-0.2 to -0.6 V) on C22.

XPS analyses

To determine film compositions, electrodes potentiostatically treated at 4 different potentials were examined by XPS; 2 potentials (0 V(+) and 0.5 V(+)) on the positive scan, and 2 (0 V(-) and -0.4 V(-)) on the negative scan. Survey spectra confirmed that the dominant bands were the Ni 2p, Cr 2p, Mo 3d, and O 1s peaks, with a peak for C 1s indicating some surface contamination. The C component was not included when determining surface compositions.

Figure 5 shows the elemental compositions (at. %) of the electrode surfaces determined from the relative intensities of the peaks in survey spectra for both alloys. As expected, the composition is dominated by the O content at all potentials. In

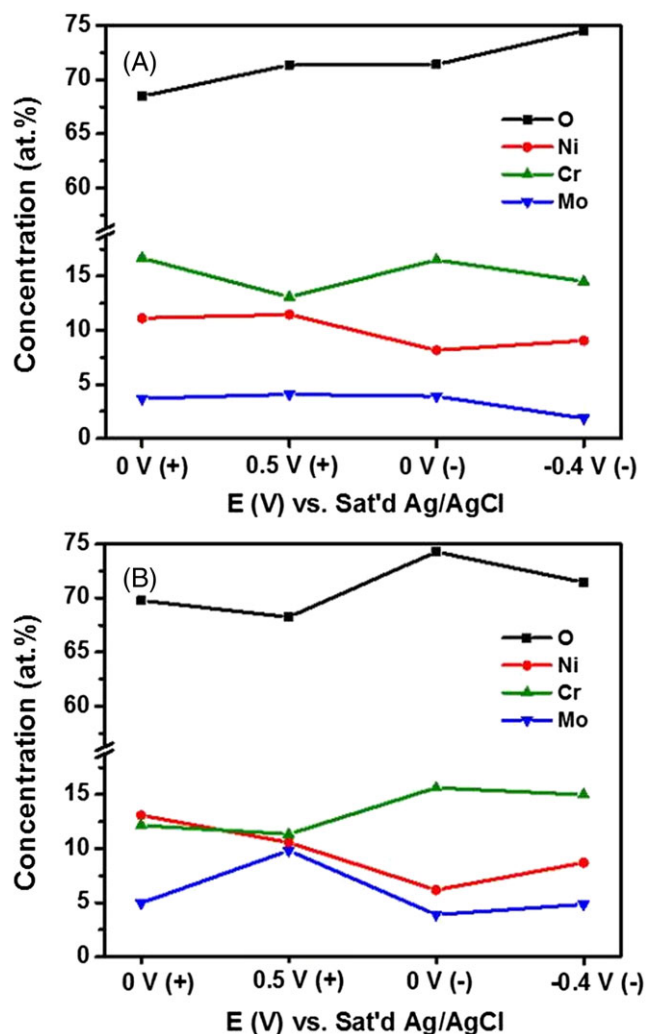


Figure 5. Surface compositions (normalized) obtained from survey spectra for A, C22 and B, BC1 after polarization at 0 and 0.5 V (0 V(+) and 0.5 V(+)) (positive-going scan) and 0 and -0.4 V (0 V(-) and -0.4 V(-)) (negative-going scan)

the passive region (0 V(+)), the surfaces of both alloys exhibit a high Cr content, especially the high Cr C22, consistent with the presence of a Cr^{III} oxide barrier layer that leads to the lower i_{Final} and higher R_f (C22) values compared to BC1. In the transpassive region (0.5 V(+)), a decrease in the relative Cr content and an increase in the relative Mo content is observed, particularly for the low Cr BC1, indicating a destruction of the passive film, at least locally, and the accumulation on the surface of Mo. Zhang et al^[5] showed that the transpassive oxidation process proceeded non-uniformly on the surface of Ni-Cr-Mo alloys.

On returning E to the passive region (0 V(-)) after a period of transpassive oxidation, the relative Cr content of the surface of both alloys was increased, with a corresponding drop in the relative Mo and Ni contents. These changes suggest the regrowth of a Cr oxide barrier layer, which would account for the high R_f values observed for both alloys on the positive-going scan at 0 V (Figure 4). For C22, the relative Cr content in the passive region (0 V) was approximately the same irrespective of the direction of the potential scan, suggesting a recovery of passivity on this alloy. For BC1, the relative Cr content was markedly higher on the negative scan, possibly indicating an improvement in passivity on this alloy. On decreasing the potential to -0.4 V(-), the relative Cr content on both alloys was maintained. That the passivity of the BC1 alloy had been improved was demonstrated by the R_f values, which were one order of magnitude greater on the negative than on the positive scan and maintained until E was reduced to < -0.4 V, Figure 4.

High-resolution spectra were collected for both alloys at the same 4 potentials. The spectra were corrected using a Shirley background subtraction and deconvoluted using the procedures developed by Biesinger et al^[27-29] and by Spevac and McIntyre.^[30] Examples of deconvoluted spectra for the O 1s, Ni 2p, Cr 2p, and Mo 3d peaks are shown in Figure 6. The deconvolution of these spectra yielded the distribution (at. %) of each component for the main alloying elements. Multiplying this by the normalized relative amounts of the main alloying elements obtained from the survey scans yielded the normalized relative film compositions plotted in Figure 7.

The oxide grown in the passive region (0 V(+)) exhibited the expected characteristics for passive films formed on Ni-Cr-Mo alloys^[4,5]: a substantial Cr_2O_3 content located at the alloy/film interface and a relatively small Mo content, indicating the presence at the oxide/solution interface of a segregated Mo-containing layer.

The detection of substantial amounts of unoxidized metal confirms that the oxide was only a few nanometres thick, as expected for a passive film.^[4,5] The presence of relatively large amounts of $\text{Ni}(\text{OH})_2$ is also expected in the outer regions of the film. The high $\text{Cr}(\text{OH})_3$ content is thought to reflect the cathodic treatment of the surface prior to applying the potential 0 V(+).^[4]

On both alloys, the signals for the unoxidized metals were significantly decreased on increasing E from the passive region (0 V(+)) to the transpassive region (0.5 V(+)), consistent with an increase in oxide film thickness, as observed previously.^[5] This was accompanied by a very significant decrease in the relative Cr_2O_3 content, indicating the destruction of the barrier layer oxide. This increase in E also led to a large increase in the Ni^{II} and Cr^{III} contents of the hydroxides present at the film/solution interfaces of both alloys. This apparent conversion of Cr^{III} in the oxide barrier layer to Cr^{III} in the outer hydroxide layer and the absence of any detectable Cr^{VI} in the film has been attributed to 1 or both of 2 possibilities: (1) the loss of Cr^{VI} by dissolution as CrO_4^{2-} and (2) reduction of Cr^{VI} retained on the surface to Cr^{III} when the electrode was transferred from the electrochemical cell to the UHV system of

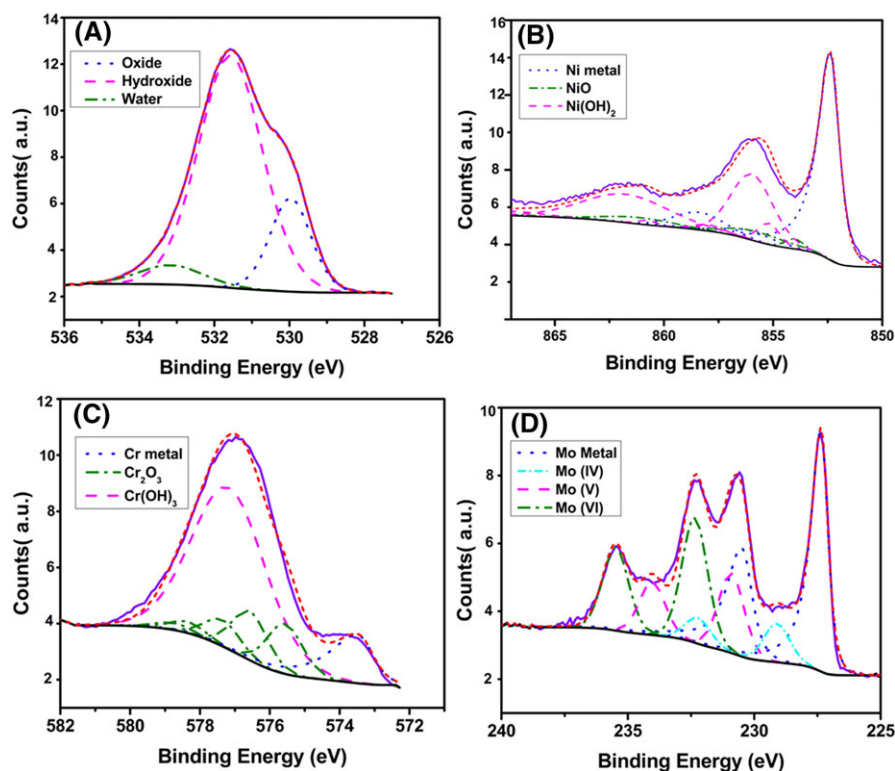


Figure 6. High-resolution deconvoluted XPS spectra for the following: A, O 1s; B, Ni 2p; C, Cr 2p; and D, Mo 3d bands collected on C22 at 0 V(+). The red lines show the fits to the spectra

the spectrometer.^[31] The relative Mo content of the surface changed only marginally on C22 when the potential was increased from the passive (0 V(+)) to the transpassive (0.5 V(+)) region. For BC1, the destruction of the Cr_2O_3 barrier layer was clearly accompanied by the formation of a Mo^{VI} layer. The extent to which the Cr_2O_3 layer on this alloy was destroyed was difficult to assess since the photoelectrons escaping from this layer at the oxide/alloy interface could have been limited by the presence of the more extensive formation (compared to C22) of the Mo^{VI} layer at the oxide/solution interface. However, the presence of a very large $\text{Cr}(\text{OH})_3$ content in the film, Figure 7B, suggested extensive degradation leading to the oxidation of large amounts of Cr to Cr^{III} , which would have been analyzed as Cr^{III} , as discussed above.

On reversing the potential (from 0.5 V (+) back to 0 V(−)), the relative Cr_2O_3 content of the film is markedly increased. This indicates that the re-formation of the protective Cr^{III} barrier layer is the dominant factor in re-establishing a high film resistance. The observation that $R_f(\text{C22})$ is approximately one order of magnitude greater at 0 V(−) after the excursion to the transpassive region (0.5 V(+)) suggests that some contribution to improved passivity is achieved by the formation of oxidized Mo surface states in the transpassive region, although this is not readily apparent in the XPS analyses.

For BC1, the relative content of Cr_2O_3 increased only marginally on decreasing E from 0.5 V(+) back to 0 V(−). While the relative surface content of the $\text{Mo}^{\text{VI}}/\text{Mo}^{\text{V}}$ states produced at 0.5 V(+) decreased somewhat, possibly due to dissolution in the neutral solution once its formation was not continued at 0.5 V(+), a significant $\text{Mo}^{\text{VI}}/\text{Mo}^{\text{V}}$ content remained on the surface. This combination of effects suggested that the re-enforced passivity on this alloy, indicated by the high value of $R_f(\text{BC1})$, was maintained dominantly by the $\text{Mo}^{\text{VI}}/\text{Mo}^{\text{V}}$ layer, rather than a regrowth of the

Cr_2O_3 barrier layer. Alternatively, the apparently small amount of Cr_2O_3 detected could reflect the disguise of a more extensive re-formation by decreased photoelectron emission due to shielding by the surface Mo^{VI} layer.

On further decreasing E to −0.4 V(−), very little change in the composition of the oxide was observed on BC1, and $R_f(\text{BC1})$ remained high, Figure 4, consistent with protection of the surface by a thin Cr_2O_3 barrier layer and a thicker outer $\text{Mo}^{\text{VI}}/\text{Mo}^{\text{V}}$ layer. By contrast, on decreasing E, the relative Cr_2O_3 content of the C22 surface was significantly decreased to a value similar to that observed in the passive region prior to the transpassive excursion (ie, at 0 V(+)). This suggests that while the Cr_2O_3 barrier layer may have reformed on returning to the passive region, the increased film resistance at 0 V(−) was predominantly due to the combined influence of the re-formed barrier layer and the Mo-rich surface layer found in the transpassive region.

Summary and conclusions

The formation, transpassive destruction, and re-formation of the passive oxide on a high Cr/low Mo (C22) and a low Cr/ high Mo (BC1) alloy were investigated electrochemically and by XPS.

On first formation, the passive film on both alloys had a similar composition, although EIS indicated that the film was more readily formed on C22 than on BC1. The lower resistance of the oxide on BC1 at the lower potential end of the passive region was attributed to the influence of Mo on the number of defects in the oxide. At more positive potentials in the passive region, the films on the 2 alloys were indistinguishable.

When oxidized in the transpassive region, the Cr^{III} barrier layer on both alloys was destroyed, at least locally, with the high Mo BC1 alloy developing a thicker Mo^{VI} layer than the low Mo C22.

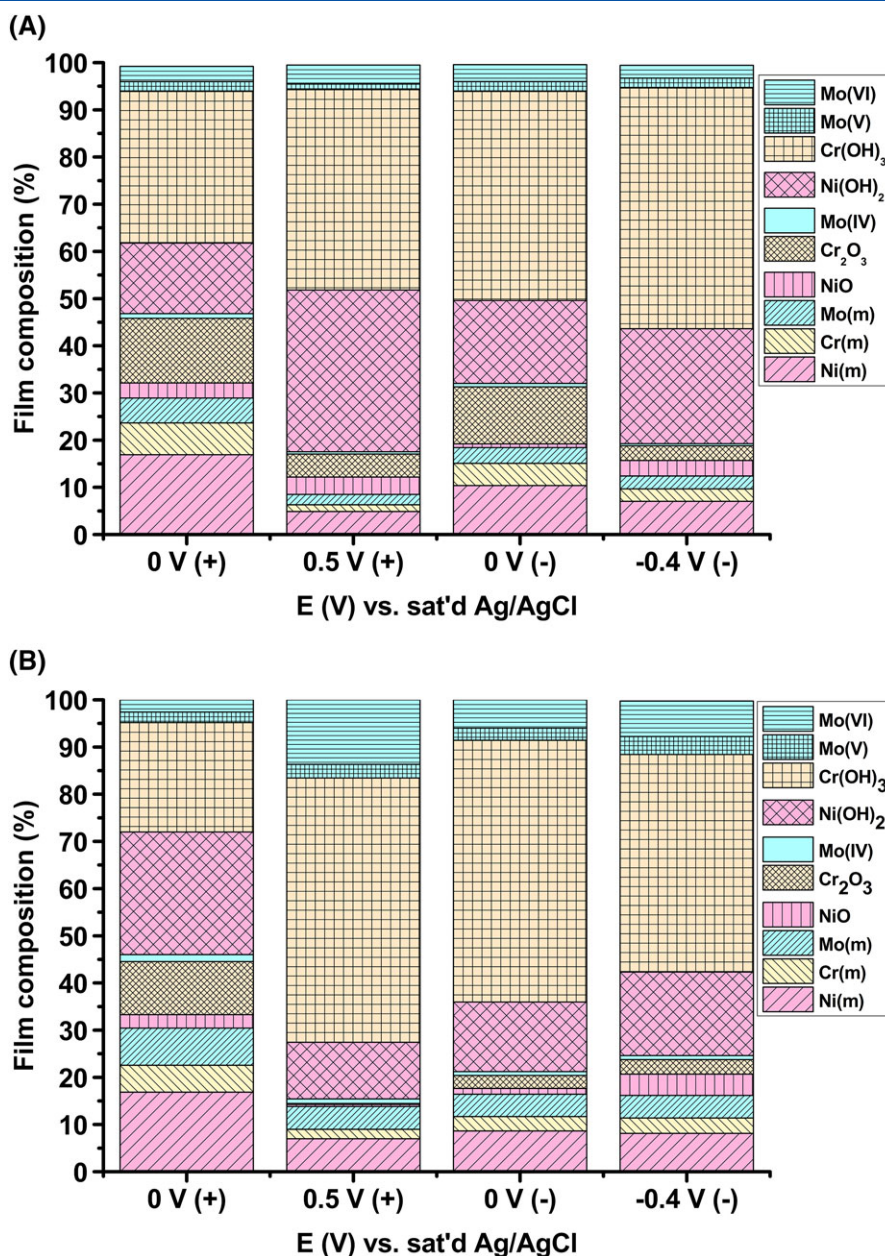


Figure 7. Normalized relative film compositions (at. %) of Ni, Cr, and Mo and their relative metal, oxide, and hydroxide components present in films polarized at the 4 potentials 0 V(+), 0.5 V(+), 0 V(-), and -0.4 V(-) (Figure 5): A, C22. B, BC1

On returning the potential to the passive region, EIS showed that the resistance of the passive oxides on both alloys was improved compared to those measured on the original passive oxides. This improvement appeared to be mainly due to the re-formation of the Cr^{III} barrier layer on C22. On BC1, the accumulated Mo^{VI} layer exerted a major influence on the improved passivity, but may have obscured an equally important contribution from a regrown Cr₂O₃ layer.

References

- [1] A. C. Lloyd, D. W. Shoesmith, N. S. McIntyre, J. J. Noël, *J. Electrochem. Soc.*, **2003**, *150*, B120–B130.
- [2] A. C. Lloyd, J. J. Noël, N. S. McIntyre, D. W. Shoesmith, *Electrochim. Acta*, **2004**, *49*, 3015–3017.
- [3] A. C. Lloyd, J. J. Noël, N. S. McIntyre, D. W. Shoesmith, *J. Metals*, **2005**, *57*, 31–35.
- [4] D. Zagidulin, X. Zhang, J. Zhou, J. J. Noël, D. W. Shoesmith, *Interface Anal.*, **2013**, *45*, 1014–1019.
- [5] X. Zhang, D. Zagidulin, D. W. Shoesmith, *Electrochim. Acta*, **2013**, *89*, 814–822.
- [6] J. J. Gray, C. A. Orme, *Electrochim. Acta*, **2007**, *52*, 2370–2375.
- [7] N. Priyantha, P. Jayaweera, D. D. Macdonald, A. Sun, *J. Electroanal. Chem.*, **2004**, *572*, 409–419.
- [8] D. D. Macdonald, A. Sun, N. Priyantha, P. Jayaweera, *J. Electroanal. Chem.*, **2004**, *572*, 421–431.
- [9] P. Jakupi, D. Zagidulin, J. J. Noël, D. W. Shoesmith, *Electrochim. Acta*, **2011**, *56*, 6251–6259.
- [10] P. Jakupi, J. J. Noël, D. W. Shoesmith, *Solid State Letts.*, **2010**, *13*, C1–C3.
- [11] N. Ebrahimi, P. Jakupi, A. Korinek, I. Barker, D. E. Moser, D. W. Shoesmith, *J. Electrochem. Soc.*, **2016**, *163*, C232–C239.
- [12] K. J. Evans, A. Yilmaz, S. D. Day, L. L. Wong, J. C. Estill, R. B. Rebak, *J. Metals*, **2005**, *57*, 56–61.

- [13] X. He, D. S. Dunn, *Corrosion*, **2007**, *63*, 145–158.
- [14] K.J. King, J.C. Estill, M.L. Stuart, G.A. Hust and R.B. Rebak, **2005**, Corrosion, Paper No. 05607, Houston, TX, NACE International.
- [15] P. Jakupi, J. J. Noël, D. W. Shoesmith, *Corros. Sci.*, **2011**, *53*, 3122–3130.
- [16] P. Jakupi, F. Wang, J. J. Noël, D. W. Shoesmith, *Corros. Sci.*, **2011**, *53*, 1670–1679.
- [17] P. Jakupi, J. J. Noël, D. W. Shoesmith, *Corros. Sci.*, **2012**, *54*, 260–269.
- [18] N. Ebrahimi, J. J. Noël, M. A. Rodriguez, D. W. Shoesmith, *Corros. Sci.*, **2016**, *105*, 58–67.
- [19] N. Ebrahimi, P. Jakupi, J. J. Noël and D.W. Shoesmith, *Corrosion*, **2015**, *71*, 1441–1451.
- [20] B. Boukamp, *J. Electrochem. Soc.*, **1995**, *142*, 1885–1894.
- [21] M. Bojinov, G. Fabricius, P. Kinnunen, T. Laitinen, K. Makela, T. Saario, G. Sundholm, *J. Electroanal. Chem.*, **2001**, *504*, 29–44.
- [22] M. Bojinov, G. Fabricius, P. Kinnunen, T. Laitinen, K. Makela, T. Saario, G. Sundholm, *Electrochim. Acta*, **2000**, *45*, 2791–2802.
- [23] B. Hirschorn, M. E. Orazem, B. Tribollet, V. Vivier, I. Frateur, M. Musiani, *ECS Trans.*, **2010**, *28(24)*, 77–94.
- [24] I. Betova, M. Bojinov, A. Englund, G. Fabricius, T. Laitinen, K. Makela, T. Saario, G. Sundholm, *Electrochim. Acta*, **2001**, *46*, 3627–3640.
- [25] M. Bojinov, G. Fabricius, T. Laitinen, K. Makela, T. Saario, G. Sundholm, *Electrochim. Acta*, **2001**, *46*, 1339–1358.
- [26] X. Zhang, Ph.D. Thesis, University of Western Ontario, London, Canada, **2012**, Chapter 4, 124–172.
- [27] M. C. Biesinger, B. Payne, A. Grosvenor, L. W. Lau, A. R. Gerson, R. S. C. Smart, *Appl. Surf. Sci.*, **2011**, *257*, 2717–2730.
- [28] M. C. Biesinger, B. Payne, L. W. Lau, A. Gerson, R. S. C. Smart, *Surf. Interface Anal.*, **2009**, *41*, 324–332.
- [29] M. C. Biesinger, C. Brown, J. Mycroft, R. D. Davidson, N. S. McIntyre, *Surf. Interface Anal.*, **2004**, *36*, 1550–1563.
- [30] P. Spevak, N. S. McIntyre, *J. Phys. Chem.*, **1992**, *96*, 9029–9035.
- [31] J. A. Bardwell, G. I. Sproule, B. MacDougall, M. J. Graham, *J. Electrochem. Soc.*, **1992**, *139*, 371–373.